Performances of metals modified activated carbons for fluoride removal from aqueous solutions

Soumia Bakhta[a,*], Zahra Sadaoui[a], Ulla Lassi[b], Henrik Romar[b], Riikka Kupila[b], Julien Vieillard[c]

[a]Laboratory of Reaction Engineering, Faculty of Mechanical and Processes Engineering, University of Sciences and Technology Houari-Boumediene, BP n°32, El alia, Bab Ezzouar, 16111 Algiers, Algeria.

[b]Research Unit of Sustainable Chemistry, University of Oulu, P.O. Box 3000, 90014 Oulu, Finland.

[c]Normandie University, ROUEN, INSA Rouen, CNRS, COBRA (UMR 6014), 55 rue Saint Germain, 27000 Évreux, France.

Abstract

The present research work focused on the activated carbon (AC) preparation from dates waste followed by its surface modification by incipient wetness impregnation using different metals: Ca, Co, Mg and Al. The obtained results showed that the AC-Al presented the best removal efficiency of the fluoride. The prepared activated carbons (AC) and (AC-Al) were characterized by several techniques. The optimization study of the AC-Al impregnation conditions was investigated by varying the impregnation time and the Al loading. Batch experiments were carried out to investigate the effect of certain operating parameters on the removal percentage. Several isotherm models were applied.

Keywords: Activated carbon; Aluminum; Incipient wetness impregnation; Adsorption; Fluoride removal.

*Corresponding author. (Soumia Bakhta)
E-mail address : soumia.bakhta64@gmail.com ; Tel.: +213 550 34 13 66

Introduction

In the region of the Algerian northern Sahara, encompassing Ouargla, Ghardaia, Touggourt, El Oued, Biskra and Hassi Messaoud, peoples in the eastern region consume groundwater from the terminal complex with a fluoride concentration above the World Health Organization standard (WHO) 1.5 $mg.L^{-1}$ [1] and will exceed 3 to 4 $mg.L^{-1}$ [2]. These waters are usually the only source for these regions [3]. The origin of the fluoride contamination in the main aquifers of the region is still not clear. In small doses in drinking water (0.5-1.5 $mg.L^{-1}$), fluoride promotes the dental and bones health. However, fluoride concentrations of 1.5 to 4 $mg.L^{-1}$ were responsible of the dental fluorosis [4] which is often appears as a change in tooth enamel, provoking dark patches [5]. This phenomenon is known as "Darmous" in the southern Algeria or " Mottled Enamel" in the Anglo-Saxon countries [2]. In addition, concentrations higher than 4 $mg.L^{-1}$, will cause the loss of the teeth and the bone fluorosis characterized by an hyper calcification of the bones. Skeletal fluorosis and possibly cancer have been diagnosed for fluoride concentrations above 10 $mg.L^{-1}$ [4]. A large percentage of inhabitants of the southern Algeria are affected by the endemic fluorosis with its two forms, dental and bone [6]. The Pasteur Institute reported this problem of the fluorosis firstly in 1932. Several surveys have been carried out, among them, those performed by the INSP (National Institute of Public Health) in 1980, which have revealed the appearance of the endemic fluorosis epidemic in the eastern part of the northern Sahara (El-Oued, Touggourt, Ouargla) [6]. This problem does not affect merely the south of Algeria, the vast region of India and some other countries such as Pakistan, Argentina, India, Korea, Russia, China, Mexico, Iran and part of Africa [7] are also affected by the high content of fluoride in the groundwater resources. Therefore, the reduction of the fluoride level in the water source at admissible concentrations is decisive to protect the public health. Many techniques have been applied for the fluoride removal from water. Several classical methods of fluoride removal

were used such as adsorption, reverse osmosis, precipitation, electrodialysis and ion exchange…etc. Adsorption has always been recommended as the cost effective and convenient method [8]. Different adsorbents were used for the fluoride removal, especially activated carbon and nanotubes, Zeolithes, activated alumina, bone char, clays and resins [8]. Among the adsorbents, activated carbon is the most used because of its high surface area, highly microporous structure and easy availability [9]. Nevertheless, activated carbon has a relatively low adsorption capacity for anionic compounds especially if they are very soluble and reactive like the fluoride. Therefore, recent investigations have focused on modifying activated carbons surface with different metal oxides and hydroxides such as Aluminum [10], Iron [8], Calcium [11], Magnesium, Manganese [12] and some rare earth metals such as Zirconium [12] and Lanthanum [8]. These investigations have proved to be interesting for enhancing significantly the fluoride adsorption efficiency. Indeed, the surface modification will lead to the formation of new functional groups on the activated carbon surface, which will have a high affinity for fluoride anions leading to the improvement of the adsorption process efficiency. The aim of the present study is to prepare an activated carbon from date stems, which is an available agricultural waste in Algeria, with its surface modification by incipient wetness impregnation using different metals (Ca, Co, Mg and Al). Indeed, fluoride has high affinity for this metals which have acceptable cost compared to the rare earth metals which are insoluble under wide pH ranges [12]. In addition, the use of the date stems is not mentioned in the literature as a precursor for fluoride adsorption. This new material's adsorption efficiency, referred by AC-Al, has been verified by its application to remove fluoride from aqueous solutions. The new material was characterized and tested for fluoride removal in batch system. Study of the impregnation conditions and the effect of certain operating parameters, in particular the contact time, the pH solution, the dose of adsorbent

and the initial concentration of fluoride on the adsorption capacity of the new material, has been tested. Isotherm analysis was also discussed.

Materials and methods

Chemicals

Zinc chloride ($ZnCl_2$) used in this study was provided from VWR Chemicals. Calcium Nitrate hydrate ($Ca(NO_3)_2,H_2O$), Cobalt Nitrate hexahydrate ($Co(NO_3)_3,6H_2O$), Magnesium Nitrate hexahydrate ($Mg(NO_3)_3,6H_2O$) and Aluminum Nitrate nonahydrate ($Al(NO_3)_3,9H_2O$) were obtained from Alfa Aesar, Germany. The Sodium fluoride (NaF, 99%) was obtained from Merck, Germany. The solution pH was adjusted by using the solution of HCl or NaOH, procured by Sigma-Aldrich. Ultrapure water (resistivity $\geq$ 18 MΩ.cm) which was produced from a Milli-Q system was used for all solutions preparations.

Preparation of the modified activated carbon

Dates stems were collected, washed, dried and crushed to get sizes smaller than 2.00 mm diameter. The sample was chemically activated using $ZnCl_2$ as dehydrating agent followed by thermal activation. For the chemical activation, about 150 g of dried precursor were mixed with the aqueous solution of $ZnCl_2$ (weight of activating agent/weight of raw material of 2/1) and stirred during 4 h at 70 °C. After the impregnation step, the sample produced was dried at 105 °C for 24 h to remove the water content. Then, the dried sample was pyrolyzed at 600 °C for 2 hours in a tubular high-temperature furnace (Nabertherm tube RT) under high purity nitrogen (99.99%) atmosphere and with a flow rate of 10 $mL.min^{-1}$. Then, the sample was cooled down to room temperature, rinsed many times with hydrochloric acid solution (0.1 M) and distilled water. Finally, the sorbent called (AC) was dried at 105°C overnight [13]. The latter was separately impregnated by different metals such as Ca, Co, Mg and Al. Metals

catalysts were prepared by incipient wetness impregnation with a metal charge of 5 (wt.%). The required amount of $Ca(NO_3)_2$,H_2O, $Co(NO_3)_26H_2O$, $Al(NO_3)_39H_2O$ and $Mg(NO_3)_36H_2O$ [14] was dissolved in a minimum volume of water. Then, the solutions were mixed neatly with 0.95 g of AC powder overnight at room temperature. The samples were rinsed with deionized water for many times to eliminate the excess of the selected cationic ions. The rinsed samples were dried overnight at 105 °C and stored in airtight bottle for the following use. The final products obtained are referred (AC-Y) where Y corresponds to the metal Ca, Co, Al and Mg.

Characterization of the adsorbent

The specific surface area and the pore size distribution of the activated carbons were determined from the nitrogen adsorption isotherms at the temperature of liquid nitrogen (77.5 K) using a Micromeritics ASAP 2020 equipment. The pore distribution was calculated from the adsorption isotherms using the density functional theory (DFT). In order to study the effect of aluminum modification on the AC structure, X-ray diffraction (XRD) studies were carried out using Bruker D8 X-ray diffractometer, with Cu K irradiation. The different bonds, present in the AC and AC-Al were determined using Fourier transformed infrared spectroscopy (FTIR). FTIR was performed using Bruker Vertex 60 at room temperature in the wave number range of 400–4000 cm^{-1}. A Field Emission Scanning Electron Microscopy (FESEM) using Zeiss Ultra Plus equipment combined with a system of analysis for energy dispersive X-ray spectroscopy EDS was used to investigate the morphology characteristics of the raw precursor and the activated carbons AC, AC-Al. The samples are coated with carbon to ensure sufficient conductivity. In addition, the elementary chemical composition of samples was obtained using an energy dispersive X-ray analyzer (EDS).XPS analysis was conducted using the ESCA-3400 Shimadzu and Al K alpha X-ray source (1486.6 eV),

although XPS pattern deconvolution was obtained with the use of a nonlinear least-square curve-fitting program (XPS-PEAK software 4.1). Zeta potential was determined using a Malvern zeta sizer nanoZS setup and the samples were prepared by dispersing 0.1 g of adsorbents in 10 mL of distilled water.

Optimization of the impregnation conditions for AC-Al

Optimal conditions for the AC-Al preparation were determined by varying the impregnation time (0.5, 1, 2, 3, 4, 24 and 48 h) and the Al loading (1, 3, 5, 7 and 10 (wt. %)). So, at room temperature, 5 g of the AC was added to an aqueous solution of $Al(NO_3)_3,9H_2O$ with known concentration and at a fixed impregnation time.Then, the product obtained was washed and dried overnight at 105 °C. The modified materials were referred as AC–AlX where X represents the aluminum content (weight percent).

Fluoride adsorption experiments

The prepared materials (modified AC) were tested for fluoride adsorption. The stock solution of fluoride was prepared by dissolving a fixed dose of the NaF salt in 1 L of pure water. All experiments were performed in batch system. 0.025 g of the modified AC was added to 25 mL of the solution with 10 $mg.L^{-1}$ of fluoride. The experiments were run in Erlenmeyer flasks, stirred in an orbital shaker at fixed speed of 125 rpm, temperature of 25 °C and pH of 6.15. The samples were carried out at equilibrium time and then filtered using syringe filters. The concentration of fluoride ions (F^-) in the adsorption experiments was checked though the fluoride ion using ion chromatographic (761 Compact IC, Metrohm). The adsorption percentage of fluoride "$R_{t,e}$"(%) and the adsorption capacity "$q_{t,e}$" ($mg.g^{-1}$) were calculated as follows:

$$R_{t,e} = \frac{(c_0 - c_{t,e})}{c_0} 100 \quad (1)$$

$$q_{t,e} = \frac{(c_0 - c_{t,e})}{m} V \quad (2)$$

Where, C_0 is the initial fluoride concentration ($mg.L^{-1}$), $C_{t,e}$ the fluoride concentration at time t or at equilibrium ($mg.L^{-1}$), V the volume of the solution (L) and m the mass of the adsorbent (g).

Results and discussion

Characterization of the adsorbent

Textural properties

The characterization results of the activated carbons AC and AC-Al5 are presented in Table 1. The table gathers surface areas, pore sizes, volumes and distributions of the pores of the prepared activated carbons. Thus, the AC without surface modification presents an important porosity that was created during the calcination step, with a high specific surface area (1341 $m^2.g^{-1}$). This value decreased for the modified activated carbon AC-Al5 (561 $m^2.g^{-1}$) suggesting a good binding of Aluminum on the AC surface. Therefore, the size and volume of the pores of the AC-Al5 were smaller than those of the AC. According to DFT model, the pore distribution results reveal that the modified activated carbon contains a higher percentage of micropores (diameter smaller than 2 nm) than the unmodified activated carbon respectively 46 and 26 %. On the other hand, a mesoporous (diameter from 2 to 50 nm) texture (74%) is predominant for the AC without modification.

X-ray diffraction studies

The XRD patterns were comparatively the same before and after impregnation, indicating the stable amorphous structure of the AC after impregnation (see Fig. 1). The XRD data analysis of the powder of the both activated carbons shows the broad noncrystalline peaks at 2θ of 25° and 43° [15].The broader reflections were found in the range of 10-30° [16]. For the AC-Al5,

no peaks corresponding to Al or any other form of Al were detected. This can be attributed to the existence of the aluminum in the amorphous phase [17].

FTIR analysis

The FTIR spectra can supply valuable information about the chemical composition of the materials. Fig.2 illustrates the apparent spectrums of the AC and AC-Al5. Thus, for the AC spectrum, the large band appearing between ~ 3600 – 2500 cm^{-1} is relating to the hydrogen bonded OH [18]. The weak peaks at 2171 and 541cm^{-1}, 2121 cm^{-1} and 2057 cm^{-1}, and 1687cm^{-1} correspond respectively to the C-O bending vibration [19,20], C≡C stretching vibrations in alkyne groups [21, 22] and C=O band of carboxylic acid [23] respectively. The sharp peak at 1562 cm^{-1} can be associated to bending vibrations of H-O-H [24] and the band at 1164 cm^{-1} can be attributed to the C–O–C stretching vibration [25]. After chemical modification of the AC, FTIR spectra were modified with apparition of new bands, while other bands disappeared, shifted or decreased in intensity. The peak at 2354 cm^{-1} can be related to OH stretch from strong H-bonded-COOH [26]. Due to Al impregnation, the band at 1562 cm^{-1} related to the H-O-H vibration shifted to 1576 cm^{-1}. Besides, the other peaks showed the small shift from 2171 to 2177 cm^{-1} (C-O) [27], from 2122 to 2119 cm^{-1} (C≡C stretching vibration) [28] and from 1687 to 1700 cm^{-1} (C=O stretch of the carboxylic acid group) [29]. The peak of 541 cm^{-1} showing C–O vibration disappeared after modification. The results indicate the appearance of peaks, which have not been identified by the unmodified activated carbon (AC) spectrum. The new bands at 1525, 1313 and 531cm^{-1} were attributed to Amide II (N-H deformation and C-N stretching) [30], Amide III (N–H, C–N) [31] and Al-O stretching vibration [32] respectively. The obtained results prove the presence of aluminum on the AC surface and can be clearly confirmed by the FESEM-EDS and XPS analysis of the AC-Al5.

Emission Scanning Electron Microscopy FESEM–EDS

The Surface morphology of the raw date stems and the activated carbons AC and AC-Al5 were investigated by FESEM and illustrated in Figs 3(a-b), 3(c-d) and 3(e-f), respectively. Contrary to the raw date stems, which exhibit rough surface morphology without porosity, the AC and AC-Al5 surfaces show clearly the well-developed pores and the complex disorganized surface structures of different open pore sizes. So, it appears that the external surface of the activated carbon is full of cavities, as the result of the chemical agent evaporation during the carbonization step, leaving the space occupied by the $ZnCl_2$ [33]. The EDS analysis was performed for both the activated carbons AC and AC-Al5. From the results gathered in Table 2, we notice that the AC includes a rich amount of C, O, and relatively median levels of inorganic components, such as Na, Si, P, S, Cl, Zn and Fe. The SEM-EDS analysis of the AC-Al5 (Table2), showed the addition of Al on the AC surface, which confirms the successful incorporation of the aluminum.

X-ray photoelectron spectrometer (XPS)

XPS analysis were used to evaluate the surface chemistry of the different AC-AlX produced. From the Fig 4.a, the peak centered at around 284.77 eV corresponds to the carbon C 1s from the C=C bond [34] and it can be also assigned to the adventitious carbon contamination from the ambient atmosphere. Although, this peak is generally referred to graphitic carbon [35]. For the AC-Al5, the peak observed at 398.94 eV from the Fig 4a, is assigned to the nitrogen N 1s and is deconvoluted, as illustrated from the Fig 4b, in three peaks associated to tertiary nitrogen $N\text{-}(C)_3$ (398.94 eV) [36], amino functional groups $R\text{-}NH_2$ (400.92 eV) [37] and oxidized nitrogen NO_2 groups (406.30 eV) [38]. Finally, from the Fig 4c, we notice that the peak at around 74.64 eV attributed to Al 2p in Al-O bond, confirmed the presence of the

aluminum (Al_2O_3 form) at the AC surface [39]. Moreover, as shown in table 3, the aluminum content loading of the AC increased from 0.32 to 1.49 % with an increase in the theoretical charge of aluminum from 1 to 10 % respectively. Finally, XPS analysis confirmed the FTIR results and the modification in aluminum content clearly affect the surface properties leading to the improvement of the fluoride adsorption capacity.

Zeta potential

Zeta potential describes the potential difference between the dispersion medium and the stationary layer of the fluid bound to the dispersed particle. It will characterize the surface charge and the acidity of the adsorbent surfaces. The negative value of the AC Zeta potential (-1.66 mV) (Fig.5) is mainly due to the presence of negative functional groups on the AC surface such as phenolic group (–OH), ketonic group (C=O) and carboxylic group (–COOH). As the fluoride ion is also negatively charged, the activated carbon surface is repelled and the adsorption capacity was limited. The zeta potential of the AC-Al5 obtained (+20.62 mV) indicates the positively charged surface, which is favorable for the fluoride adsorption by electrostatic interactions. After the fluoride adsorption, the zeta potential of the AC-Al5 had negative value (-5.91 mV) confirming that the fluoride anions were adsorbed on the AC-Al5.

Optimization of the impregnation conditions of the AC

Effect of the impregnation agent on the fluoride removal

The selectivity study was performed based on the selection of the better adsorbent, which leads to the highest fluoride adsorption. In accordance with the obtained results, the activated carbon impregnated with aluminum (AC-Al5) presented significantly better adsorption percentage (80%) compared to Ca, Mg and Co impregnated ones (5 - 15 %). As can be seen from Fig.6, an improvement of fluoride removal from 2 to 80 % was noted respectively for

the AC and AC-Al5. It is clear, from Fig.6 that the preferential chemical species impregnation for fluoride adsorption follows the order of Al > Co > Ca > Mg. This may be ascribed to the stronger specific interactions between Al^{3+} and F^- than Co^{+2} and F^-, Ca^{+2} and F^- and Mg^{2+} and F^- which will probably attributed to the number of the positive charges. In addition, aluminum could provide more active sites for complexation or ligand exchange with fluoride (such as $AlF_{3(aq)}$) compared with other metals [40].

Effect of the impregnation time on the fluoride removal

Different AC-Al5 sorbent with different impregnation times (from 0.5 to 48 h) were prepared to define the best condition of synthesis. It is clear from Fig.7 that the increase of the impregnation time from 0.5 to 2 h, leads to an enhancement in the fluoride removal from 65 to 80 % respectively. This result may be attributed to the increase of the fixed aluminum on the AC surface with impregnation time, which allows the fixation of more fluoride anions. However, the raise in impregnation time up to 2 h of contact has no significant effect on the fluoride removal, which revealed that the equilibrium state was established. Similar results have been also obtained by other studies [41]**.** Therefore, an impregnation time of 2 h is taking as the optimal value for the aluminum loading study.

Effect of the aluminum loading on the fluoride removal

The effect of Al loading on the fluoride removal efficiency was investigated within a range from 1 to 10 (wt.%). As shown in Fig. 8a, the maximum fluoride removal was achieved at a maximum value of 80 % for an Al loading of 5 % (AC-Al5 sorbent). However, a decline of the fluoride removal with a progressive increase of Al loading more than 5 % was noted. The low efficiency for both AC-Al7 and AC-Al10 will be attributed to the deficit of available active sites required for the fluoride removal related to the pore blockages [42]. Indeed,

according to the XPS analysis results, we have noted that the aluminum adsorption percentage on the AC decreased from 20 to 14 % when Al loading exceeds 5 % (Fig 8b) leading to the fluoride removal decrease.

Parametric study of the fluoride adsorption on the AC-Al5

Effect of contact time

Fig 9 presents the results obtained from the study of the effect of contact time on the fluoride removal by adsorption on the AC-Al5. The fluoride is rapidly adsorbed in the first 5 -10 min, then the adsorption increased slowly until reaching equilibrium in about 1 h. The first step of adsorption is fast, because the fluoride was adsorbed onto the external surface due to the availability of Al active sites. When the external surface is saturated, the fluoride ions are transferred to the inner surface via the pores. This interne transfer takes a relatively long contact time.

Effect of pH

Generally, the pH of the aqueous solution is an essential parameter effecting the adsorption process. For this study, the initial pH values were varied from 3 to 12 keeping constant all other parameters (adsorbent mass =1g, $[F^-]_o$ = 10 mg.L^{-1} and T = 25 °C). From the results presented in Fig. 10a, we note that the fluoride removal percentage was high (85 %) and stable within a pH range from 5 to 10. Hence, this result is useful for its use for the wastewater treatment, which generally has a wide range of pH levels, ranging between 6 and 9. For pH values lower than 5 or higher than 10, the removal efficiency fell sharply. Allalou and al., obtained similar results for the nitrate adsorption onto surfactant modified activated

carbon [13]. The significant decrease of the fluoride removal for alkaline pH is possibly due to the competition between fluoride anions (F^-) and hydroxyl ions (OH^-) on the adsorbent surface. In the other hand, below pH 5, the efficiency removal decrease may be attributed to the protonation of the fluoride ion and the formation of weakly ionized hydrofluoric acid. Such results are consistent with the results of other researchers who investigated the fluoride adsorption on other activated carbons [43]. In other hand, the equilibrium pH values were measured after fluoride adsorption on the AC-Al5 at different initial pH values (Figure 10b). Upon adsorption experiments, the pH equilibrium values significantly decreased for the initial pH values between 5–10. The results showed that the effective initial pH for fluoride removal was between 5 and 10 in this study. In view of the effective and stable rate of defluoridation and the free pH of the fluoride solution (around 6.15), there was no further adjustment of the solution pH, for the following experiments.

Effect of the adsorbent dose

The adsorbent dose has a significant impact on the adsorption process. The effect of this parameter on the fluoride removal was shown in the Fig.11 within a range from 0.2 to 4 $g.L^{-1}$. The initial fluoride concentration and solution pH were fixed respectively to 10 $mg.L^{-1}$ and 6.15. In accordance with the Fig.11, the fluoride removal percentage increased significantly from 29 to 90 % when the adsorbent level rises from 0.2 to 1.5 $g.L^{-1}$.This may be explained by the fact that the active sites availability increases with the adsorbent amounts leading to the improvement of the fluoride adsorption. Furthermore, the fluoride removal was almost constant when the adsorbent dose was higher than 1.5 $g.L^{-1}$. This result may be attributed to the overlapping of the active sites at higher doses and thus the effective surface area decreases [15].

Effect of the fluoride initial concentration and isotherms modeling

The effect of the initial fluoride concentration on the adsorption process was performed for the concentrations ranging from 5 to 30 mg.L^{-1} at ambient temperature (25 °C), free pH and adsorbent dose of 1.5 g.L^{-1}. As shown in Fig.12, the fluoride removal efficiency decreased from 94 to 57 % by increasing the initial concentration of fluoride from 5 to 30 mg.L^{-1}. The decrease in fluoride adsorption will be due to the deficit of the active sites needed for the high fluoride initial concentrations. The better efficiency in fluoride removal, at low levels, is related with the availability of active sites for less fluoride ions on the adsorbent surface [43]. The equilibrium is established during adsorption between the amount of fluoride adsorbed on the adsorbent (q_e) and the fluoride remaining in solution (C_e). The isothermal data of the adsorption are primarily important to predict the adsorption process. Several nonlinear isotherms models such as the two parameters (Langmuir, Freundlich and Temkin) and the three-parameters (Sips and Redlich–Peterson) adsorption models were used to study the equilibrium isotherms of fluoride adsorption on the AC-Al5. The equilibrium adsorption isotherms were investigated through the application of Langmuir (Eq. 3), Freundlich (Eq. 5) and Temkin (Eq. (6), Sips (7) and Redlich–Peterson (8) equations.

The Langmuir theory suggests that the adsorbate covers a monolayer over a homogeneous adsorbent surface. The Langmuir equation is expressed as follow:

$$q_e = \frac{q_{\max} K_L C_e}{(1 + K_L C_e)} \qquad (3)$$

q_e (mg.g^{-1}) is the fluoride adsorption capacity at equilibrium, $q_{\max}$ (mg.g^{-1}) the theoretical maximum adsorption capacity, C_e (mg.L^{-1}) the equilibrium fluoride concentration and K_L

($L.mg^{-1}$) the Langmuir constant. Another essential parameter of the model is a dimensionless constant known as the Webber and Chakkravorti Separation Factor (R_L):

$$R_L = \frac{1}{(1+K_L C_e)} \quad (4)$$

A more profound interpretation reveals that the R_L value indicates either unfavorable adsorption (R_L>1), linear (R_L=1), favorable (0 <R_L< 1) or irreversible (R_L=0). The Freundlich equation is an empirical equation, which indicates that molecules are adsorbed on heterogeneous surfaces in mono or multi layers and can be expressed as:

$$q_e = K_F C e^{1/n_F} \quad (5)$$

K_F [($mg.g^{-1}$) ($mg.L^{-1}$)$^{-1/n}$] is the Freundlich constant and n_F, the heterogeneity factor. The n_F values > 1 reflect favorable adsorption conditions [44]. The Temkin isotherm is based on an indirect interaction adsorbate/adsorbent and is represented with the following equation:

$$q_e = B \ln(A_T C_e) \quad (6)$$

Where, $B = \frac{RT}{b_T}$ and b_T ($J.mol^{-1}$) is the Temkin constant associated with the adsorption heat and A_T, the equilibrium bond constant ($L.g^{-1}$), R (8.314 $J.mol^{-1}.K^{-1}$) is the gas constant, T (K), the absolute temperature. The nonlinear Sips isotherm is the combination of Langmuir and Freundlich isotherms. The equation of the model is given as follow:

$$q_e = \frac{(q_s K_s C_e^{n_s})}{(1+K_S C_e^{n_s})} \quad (7)$$

q_s, K_S and n_S are the Sips constants. K_S ($L.g^{-1}$) is related to the adsorption energy and n_s reveals the heterogeneity of the system. The Redlich–Peterson isotherm contained three adjustable parameters into an empirical isotherm. This equation is commonly used like a

compromise between Langmuir and Freundlich systems as illustrated in the following expression:

$$qe = \frac{K_{RP} C_e}{(1 + a_R C_e^{\beta})} \quad (8)$$

K_{RP}, a_R and β are the Redlich–Peterson isotherm constants, where, $0 \ll \beta \ll 1$.

Error Functions

A variety of error functions is available in the literature to evaluate the validity of the adsorption isotherms models with the experimental data. Indeed, the only use of the regression coefficient R^2 is not enough for isothermal data analysis, since the experiment results may have high R^2. Consequently, the result for the residue analysis must be diagnosed. In this study, the residual root mean square error (RMSE) and the Reduced Chi-squared (χ^2_{red}) were introduced in order to evaluate the fit of the isotherms equations to the experimental results. The smaller the error value, the more suit the curve fit. The calculated error functions expressions can be described as :

$$RMSE = \sqrt{(\frac{1}{N-p}) \sum_{i=1}^{N} (q_{i,\exp} - q_{i,cal})^2} \quad (9)$$

$$\chi^2_{red} = \sum_{i=1}^{N} \frac{(q_{i,\exp} - q_{i,cal})^2}{N - P} \quad (10)$$

Where N is the number of data experimental points, p is the number of isotherm model parameters, $q_{i,exp}$ is the q_i experimental value, $q_{i,cal}$, the q_i value estimated by the isotherm model. The graphs using the non-linearized isotherm models equations are shown in Fig.13. Table 4 gathered the different constants of the five isotherm models, R^2, RMSE and Reduced Chi-squared (χ^2_{red}) values. The results obtained for the application of the two parameters

isotherm models, showed clearly that the Temkin and Langmuir models were more suitable to fit the experimental data than the freundlich model with the lowest values for the error functions. The q_{max} and K_L values estimated from the Langmuir equation were 13.03 $mg.g^{-1}$ and 0.91 $L.mg^{-1}$, respectively. Additionally, the R_L values are inside the validity range, indicating the favorable fluoride adsorption on the AC-Al5 (Table 5). The obtained values of the Temkin parameters A_T=11.61 $L.g^{-1}$ and B = 0.0025 $kJ.mol^{-1}$, indicate that the fluoride adsorption on the AC-Al5 occurred by physisorption. The bonding energy value, which is < 8 $kJ.mol^{-1}$, confirmed this mechanism. Moreover, as indicated in table 4, the value of the Freundlich parameter "n_F" is higher than 1, indicating the favorable adsorption. Otherwise, the three parameters isotherm models R-P and Sips, provide a good fit (R^2 = (0.97, R^2 = 0.96), RMSE = (0.584, 0.636) and χ^2_{red} = (0.3414, 0.405)), respectively. Hence, the R-P and sips models combine the expressions of Langmuir and Freundlich and it is generally known to represent well the adsorption on heterogeneous surfaces. In comparison with previous data already published in literature, the fluoride adsorption capacity of the AC-Al5 sorbent was much better than other adsorbents (Table 6).

Conclusion

A novel material laws successfully produced by surface modification of an activated carbon prepared from date stems by fixing different metals: Ca, Co, Mg and Al onto the activated carbon (AC) surface. Indeed, the surface modification applied to the produced activated carbon had a positive effect on the fluoride removal efficiency from water. The highest fluoride removal was obtained for Al compared to the others impregnated metals. From the characterization results of the AC-Al5, it was observed that aluminum is principally present in the form of Al_2O_3. Furthermore, the results of the nitrogen adsorption volumetric analysis reveal BET surface areas of 1341 $m^2.g^{-1}$ and 561 $m^2.g^{-1}$ respectively for the AC and AC-Al5,

suggesting a good fixation of aluminum on the AC surface. On the other hand, the fluoride removal was found to be dependent on the impregnation operating parameters. The optimal removal (80 %) was achieved for the impregnation time = 2 h and aluminum loading = 5 (wt. %). The adsorption experimental results showed that fluoride adsorption on the AC-Al5 was rapid and reached the equilibrium within 1 h of contact time. In addition, the fluoride removal efficiency was found to be dependent on the operating parameters (initial solution pH, AC-Al dose and initial fluoride concentration).On the other hand, this study shows that the fluoride adsorption efficiency is independent of the solution pH in the wide range of pH values (5.0 - 11.0). The Langmuir, Temkin, Sips and Redlich-Peterson isotherm models fit adequately the experimental data. The q_{max} value estimated from the Langmuir model was found to be equal to 13.03 $mg.g^{-1}$. The results of the present study revealed that the produced AC-Al5 is a promising material for the water treatment by removing anionic compounds particularly fluoride.

References

[1] World Health Organization, Guidelines for Drinking-water Quality, 2019.

[2] S. Achour, L. Youcef, Defluoruration des eaux du Sahara septentrional Algerien par adsorption sur des bentonites locales, Int. J. Environ. Stud. 66 (2009) 151–165. doi:10.1080/00207230902859747.

[3] L. Youcef , S. Achour, Defluoruration des eaux souterraines du sud Algerien par la chaux et le sulfate d'aluminium, Courrier du Savoir .1 (2001) 65–71.

[4] D.L. Ozsvath, Fluoride and environmental health: A review, Rev. Environ. Sci. Biotechnol. 8 (2009) 59–79. doi:10.1007/s11157-008-9136-9.

[5] Chetan P. S. Ahada1 · Surindra Suthar1, Assessment of Human Health Risk Associated

with High Groundwater Fluoride Intake in Southern Districts of Punjab , India, Expo. Heal. (2017). doi:10.1007/s12403-017-0268-4.

[6] L. Youcef, Elimination de polluants minéraux des eaux par des procédés physico-chimiques de précipitation et d'adsorption, (2006). PhD thesis in hydraulic sciences, Mohamed Khider University –Biskra, pp 9. http://thesis.univ-biskra.dz/2720/.

[7] M. Ghaderpoori, M. Paydar, A. Zarei, H. Alidadi, A.A. Najafpoor, A.H. Gohary, M. Shams, Health risk assessment of fluoride in water distribution network of Mashhad, Iran, Hum. Ecol. Risk Assess. 25 (2018) 851–862. doi:10.1080/10807039.2018.1453297.

[8] A.Mullick, S. Neogi, Acoustic cavitation induced synthesis of zirconium impregnated activated carbon for effective fluoride scavenging from water by adsorption, Ultrason. Sonochem. 45 (2018) 65–77. doi:10.1016/j.ultsonch.2018.03.002.

[9] A. Bhatnagar, W. Hogland, M. Marques, M. Sillanpää, An overview of the modification methods of activated carbon for its water treatment applications, Chem. Eng. J. 219 (2012) 499–511. doi:10.1016/j.cej.2012.12.038.

[10] Y.H. Li, S. Wang, A. Cao, D. Zhao, X. Zhang, C. Xu, Z. Luan, D. Ruan, J. Liang, D. Wu, B. Wei, Adsorption of fluoride from water by amorphous alumina supported on carbon nanotubes, Chem. Phys. Lett. 350 (2001) 412–416. doi:10.1016/S0009-2614(01)01351-3.

[11] S. Roy, P. Das, S. Sengupta, S. Manna, Calcium impregnated activated charcoal: Optimization and efficiency for the treatment of fluoride containing solution in batch and fixed bed reactor, Process Saf. Environ. Prot. 109 (2017) 18–29. doi:10.1016/j.psep.2017.03.026.

[12] A. Mullick, S. Neogi, Ultrasound assisted synthesis of Mg-Mn-Zr impregnated activated carbon for effective fluoride adsorption from water, Ultrason. Sonochem. 50

(2018) 126–137. doi:10.1016/j.ultsonch.2018.09.010.

[13] O. Allalou, D. Miroud, M. Belmedani, Z. Sadaoui, Performance of surfactant-modified activated carbon prepared from dates wastes for nitrate removal from aqueous solutions, Environ. Prog. Sustain. Energy. 38 (2018) S403–S411. doi:10.1002/ep.13090.

[14] M.C. Macías-Pérez, A. Bueno-López, M.A. Lillo-Ródenas, C. Salinas-Martínez de Lecea, A. Linares-Solano, SO2 retention on CaO/activated carbon sorbents. Part I: Importance of calcium loading and dispersion, Fuel. 86 (2007) 677–683. doi:10.1016/j.fuel.2006.09.004.

[15] R. Araga, S. Soni, C.S. Sharma, Fluoride adsorption from aqueous solution using activated carbon obtained from KOH-treated jamun (Syzygium cumini) seed, J. Environ. Chem. Eng. 5 (2017) 5608–5616. doi:10.1016/j.jece.2017.10.023.

[16] Q.L. Shimabuku, F.S. Arakawa, M. Fernandes Silva, P. Ferri Coldebella, T. Ueda-Nakamura, M.R. Fagundes-Klen, R. Bergamasco, Water treatment with exceptional virus inactivation using activated carbon modified with silver (Ag) and copper oxide (CuO) nanoparticles, Environ. Technol. (United Kingdom). 38 (2016) 2058–2069. doi:10.1080/09593330.2016.1245361.

[17] S.Kalidindi, M.Vecha, A.Kar, and T. Raychoudhury, Aluminum – cerium double-metal impregnated activated carbon : a novel composite for fl uoride removal from aqueous solution Shreeya Kalidindi , Mounica Vecha , Arkamitra Kar and Trishikhi Raychoudhury, (2017) 115–124. doi:10.2166/ws.2016.114.

[18] J. Shu, R. Liu, Z. Liu, H. Chen, C. Tao, Simultaneous removal of ammonia and manganese from electrolytic metal manganese residue leachate using phosphate salt, J. Clean. Prod. 135 (2016) 468–475. doi:10.1016/j.jclepro.2016.06.141.

[19] F. Cataldo, M. V. Putz, O. Ursini, G. Angelini, Surface modification of activated

carbon fabric with ozone. Part 2: Thermal analysis with TGA-FTIR and DTA, Fullerenes Nanotub. Carbon Nanostructures. 24 (2016) 400–405. doi:10.1080/1536383X.2016.1172068.

[20] N.S. Kumar, K. Min, Phenolic compounds biosorption onto Schizophyllum commune fungus: FTIR analysis, kinetics and adsorption isotherms modeling, Chem. Eng. J. 168 (2011) 562–571. doi:10.1016/j.cej.2011.01.023.

[21] H.A. Hasan, S.R.S. Abdullah, N.T. Kofli, S.K. Kamarudin, Isotherm equilibria of Mn^{2+} biosorption in drinking water treatment by locally isolated Bacillus species and sewage activated sludge, J. Environ. Manage. 111 (2012) 34–43. doi:10.1016/j.jenvman.2012.06.027.

[22] T. Yang, A.C. Lua, Characteristics of activated carbons prepared from pistachio-nut shells by physical activation, J. Colloid Interface Sci. 267 (2003) 408–417. doi:10.1016/S0021-9797(03)00689-1.

[23] K. Chullasat, P. Nurerk, P. Kanatharana, F. Davis, O. Bunkoed, A facile optosensing protocol based on molecularly imprinted polymer coated on CdTe quantum dots for highly sensitive and selective amoxicillin detection, Sensors Actuators, B Chem. 254 (2018) 255–263. doi:10.1016/j.snb.2017.07.062.

[24] A.L. Smirnov, S.Y. Skripchenko, V.N. Rychkov, M.G. Shtutsa, L.A. Plotnikov, E.S. Koparulina, A.M. Pastukhov, Preparation conditions effect on the properties of uranium tetrafluoride, Theor. Found. Chem. Eng. 48 (2014) 502–508. doi:10.1134/S0040579514040113.

[25] A. Heidari, H. Younesi, A. Rashidi, A.A. Ghoreyshi, Evaluation of CO2 adsorption with eucalyptus wood based activated carbon modified by ammonia solution through heat treatment, Chem. Eng. J. 254 (2014) 503–513. doi:10.1016/j.cej.2014.06.004.

[26] C. Lu, C. Liu, G.P. Rao, Comparisons of sorbent cost for the removal of Ni^{2+} from

aqueous solution by carbon nanotubes and granular activated carbon, J. Hazard. Mater. 151 (2008) 239–246. doi:10.1016/j.jhazmat.2007.05.078.

[27] T. Kaljuvee, M. Keelman, A. Trikkel, V. Petkova, TG-FTIR/MS analysis of thermal and kinetic characteristics of some coal samples, J. Therm. Anal. Calorim. 113 (2013) 1063–1071. doi:10.1007/s10973-013-2957-y.

[28] A. Bodaghi, M. Shahidzadeh, Synthesis and Characterization of New PGN Based Reactive Oligomeric Plasticizers for Glycidyl Azide Polymer, Propellants, Explos. Pyrotech. 43 (2018) 364–370. doi:10.1002/prep.201700219.

[29] L. Wang, J. Zhang, R. Zhao, Y. Li, C. Li, C. Zhang, Adsorption of Pb(II) on activated carbon prepared from Polygonum orientale Linn.: Kinetics, isotherms, pH, and ionic strength studies, Bioresour. Technol. 101 (2010) 5808–5814. doi:10.1016/j.biortech.2010.02.099.

[30] N. Chubar, T. Behrends, P. Van Cappellen, Biosorption ofmetals (Cu^{2+},Zn^{2+}) and anions (F^{-},$H_2PO_4^{-}$) by viable and autoclaved cells of the Gram-negative bacterium Shewanella putrefaciens, 65 (2008) 126–133. doi:10.1016/j.colsurfb.2008.03.006.

[31] S.R. Shanmugam, S. Adhikari, Z. Wang, R. Shakya, Treatment of aqueous phase of bio-oil by granular activated carbon and evaluation of biogas production, Bioresour. Technol. 223 (2017) 115–120. doi:10.1016/j.biortech.2016.10.008.

[32] T.Y. Datsko, V.I. Zelentsov, E.E. Dvornikova, Physicochemical and adsorption-structural properties of diatomite modified with aluminum compounds, Surf. Eng. Appl. Electrochem. 47 (2011) 530–539. doi:10.3103/S1068375511060081.

[33] H. Deng, L. Yang, G. Tao, J. Dai, Preparation and characterization of activated carbon from cotton stalk by microwave assisted chemical activation-Application in methylene blue adsorption from aqueous solution, J. Hazard. Mater. 166 (2008) 1514–1521. doi:10.1016/j.jhazmat.2008.12.080.

[34] H.J. Niu, L. Zhang, J.J. Feng, Q.L. Zhang, H. Huang, A.J. Wang, Graphene-encapsulated cobalt nanoparticles embedded in porous nitrogen-doped graphitic carbon nanosheets as efficient electrocatalysts for oxygen reduction reaction, J. Colloid Interface Sci. 552 (2019) 744–751. doi:10.1016/j.jcis.2019.05.099.

[35] R. Chen, L. Li, Z. Liu, M. Lu, C. Wang, H. Li, W. Ma, S. Wang, Preparation and characterization of activated carbons from tobacco stem by chemical activation, J. Air Waste Manag. Assoc. 67 (2017) 713–724. doi:10.1080/10962247.2017.1280560.

[36] Y. Tan, Z. Shu, J. Zhou, T. Li, W. Wang, Z. Zhao, One-step synthesis of nanostructured g-C3N4/TiO2 composite for highly enhanced visible-light photocatalytic H2 evolution, Appl. Catal. B Environ. 230 (2018) 260–268. doi:10.1016/j.apcatb.2018.02.056.

[37] F. Gong, J. Zhang, L. Ding, Z. Yang, X. Liu, Mussel-inspired coating of energetic crystals : a compact core-shell structure with highly enhanced thermal stability, Chem. Eng. J. (2016). doi:10.1016/j.cej.2016.10.020.

[38] T.B. and J.G. B. Anothumakkoola, P-Louis Tabernab, B.Daffosb, P.Simonb, Y- S-A.Barazaa, C.Ewelsa, Improved electro-grafting of nitropyrene onto onion-like carbon via in situ electrochemical reduction and polymerization: Tailoring redox energy density of the supercapacitor positive electrode, (2016). doi:10.1039/C6TA08170C.

[39] A. Philip, S. Thomas, K.R. Kumar, Compositional characterization of atomic layer deposited alumina, AIP Conf. Proc. 1576 (2014) 183–185. doi:10.1063/1.4862015.

[40] C. Huang, H. Zhang, W. Zeng, J. Ma, S. Zhao, Enhanced fluoride adsorption of aluminum humate and its resistance on fluoride accumulation in tea leaves, Environ. Technol. 41 (2018) 329-338. doi:10.1080/09593330.2018.1498135.

[41] S. Jagtap, M.K. Yenkie, S. Das, S. Rayalu, Synthesis and characterization of lanthanum impregnated chitosan flakes for fluoride removal in water, Desalination. 273 (2011)

267–275. doi:10.1016/j.desal.2010.12.032.

[42] E. Vences-Alvarez, L.H. Velazquez-Jimenez, L.F. Chazaro-Ruiz, P.E. Diaz-Flores, J.R. Rangel-Mendez, Fluoride removal in water by a hybrid adsorbent lanthanum-carbon, in: J. Colloid Interface Sci., Elsevier Inc, 455 (2015). 194–202. doi:10.1016/j.jcis.2015.05.048.

[43] G. Wendimu, F. Zewge, E. Mulugeta, Aluminium-iron-amended activated bamboo charcoal (AIAABC) for fluoride removal from aqueous solutions, J. Water Process Eng. 16 (2016) 123–131. doi:10.1016/j.jwpe.2016.12.012.

[44] C.S.T. Araújo, I.L.S. Almeida, H.C. Rezende, S.M.L.O. Marcionilio, J.J.L. Léon, T.N. de Matos, Elucidation of mechanism involved in adsorption of Pb(II) onto lobeira fruit (Solanum lycocarpum) using Langmuir, Freundlich and Temkin isotherms, Microchem. J. 137 (2017) 348–354. doi:10.1016/j.microc.2017.11.009.

[45] L. Mei, H. Qiao, F. Ke, C. Peng, R. Hou, X. Wan, H. Cai, One-step synthesis of zirconium dioxide-biochar derived from Camellia olei- fera seed shell with enhanced removal capacity for fluoride from water, Appl. Surf. Sci. 509 (2019) 144685. doi:10.1016/j.apsusc.2019.144685.

[46] N.K. Mondal, R. Bhaumik, J.K. Datta, Removal of fluoride by aluminum impregnated coconut fiber from synthetic fluoride solution and natural water, Alexandria Eng. J. 54 (2015) 1273–1284. doi:10.1016/j.aej.2015.08.006.

[47] M.A.S.C. R.Leyva.Ramos,J.O.Turrubiartes, adsorption of fluoride from aqueous solution on aluminum-impregnated carbon, Carbon.37 (1999) 609-617. doi.org/10.1016/S0008-6223(98)00231-0.

Table 1. Surface area, pore volume, pore size and pore distribution of the AC and AC-Al5.

	BET			DFT pore distribution		
Sample	Surface area ($m^2.g^{-1}$)	Pore volume ($cm^3.g^{-1}$)	Pore size(nm)	Micropores (%)	Mesopores (%)	Macropores (%)
AC	1342	1.213	3.488	26	74	0
AC-Al5	561	0.392	2.742	46	54	0

Table 2. EDS analysis of AC and AC-Al5

Sample	**C** (wt. %)	**O** (wt. %)	**Al** (wt. %)	**Si** (wt. %)	**P** (wt. %)	**S** (wt. %)	**Cl** (wt. %)	**Zn** (wt. %)	**Fe** (wt. %)	**Na** (wt. %)	**Mg** (wt. %)
AC	71.37	15.53	-	0.38	0.13	0.48	1.05	7.75	2.52	0.78	-
AC-Al5	34.04	33.85	**20.11**	0.67	0.34	0.92	2.73	5.57	1.01	-	0.76

Table 3. XPS analysis of the aluminum-modified activated carbon (AC-Al) with different Al loading.

Sample	**Elemental composition (wt. %)**						
	C 1s	**O 1s**	**Al 2p**	**N 1s**	**N 1s A**	**N 1s B**	**Cl 2p**
AC-Al1	91.10	7.26	0.32	0.35	0.36	0.23	0.39
AC-Al3	87.98	9.55	0.72	0.32	0.36	0.66	0.41
AC-Al5	84.78	12.07	1.02	0.35	0.45	0.89	0.44
AC-Al7	83.19	13.21	1.16	0.37	0.38	1.23	0.47
AC-Al10	80.91	15.03	1.49	0.34	0.37	1.48	0.39

Table 4. The Langmuir, Freundlich, Temkin, Sips and Redlich– Peterson parameters of the fluoride adsorption isotherms.

Isotherm models	Parameters	Values
Langmuir	R^2	0.972
	RMSE	0.581
	χ^2_{red}	0.337
	q_{max} ($mg.g^{-1}$)	13.031
	K_L	0.912
Freundlich	R^2	0.931
	RMSE	0.908
	χ^2_{red}	0.825
	n_F	3.309
	K_F	6.071
Temkin	R^2	0.977
	RMSE	0.525
	χ^2_{red}	0.276
	A_T ($L.mg^{-1}$)	11.614
	b_T ($J.mol^{-1}$)	979.436
Sips	R^2	0.966
	RMSE	0.636
	χ^2_{red}	0.405
	q_s	13.932
	K_s	0.798
	n_s	0.851
Redlich– Peterson	R^2	0.971
	RMSE	0.584
	χ^2_{red}	0.341
	K_{RP}	15.81
	a_R	1.524
	β	0.905

Table 5. Separation factor for different initial concentrations of fluoride.

C_0 ($mg.L^{-1}$)	5	10	15	20	25	30
R_L	0.7633	0.5061	0.3541	0.1798	0.1099	0.0872

Table 6. Adsorption capacities for fluoride using different adsorbents.

Adsorbents	q_{max} ($mg.g^{-1}$)	References
AC-Zr	5.4	[8]
Lanthanum–carbon	9.98	[42]
Aluminum–cerium double-metal impregnated activated carbon	3.05	[17]
Zirconium-impregnated Camellia seed biochar	11.04	[45]
Aluminum impregnated coconut fiber ash	3.192	[46]
Aluminum impregnated carbon	1.07	[47]
Aluminum–modified activated carbon (AC-Al) from dates stems	13.03	**This study**

Figure

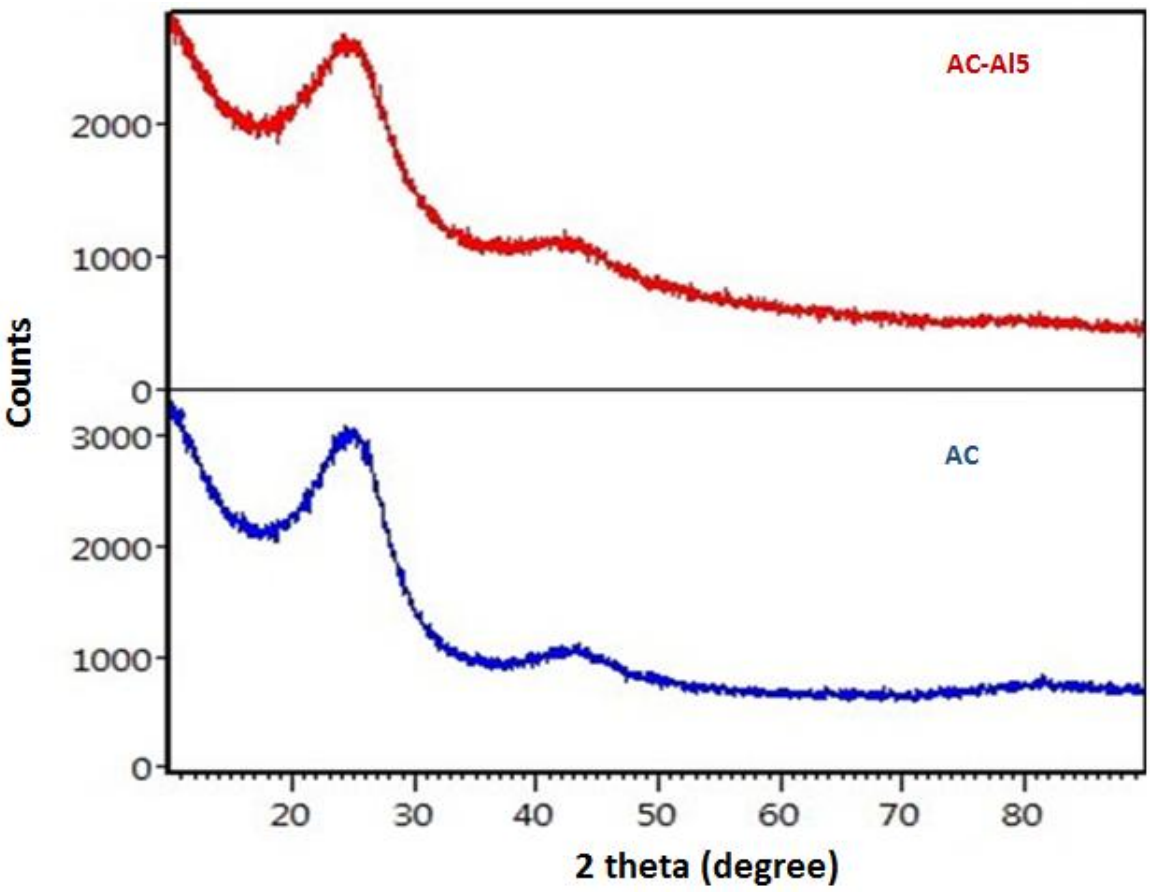
AC-Al5
AC
Counts
2000
1000
0
3000
2000
1000
0
20
30
40
50
60
70
80
2 theta (degree)

Fig. 1.

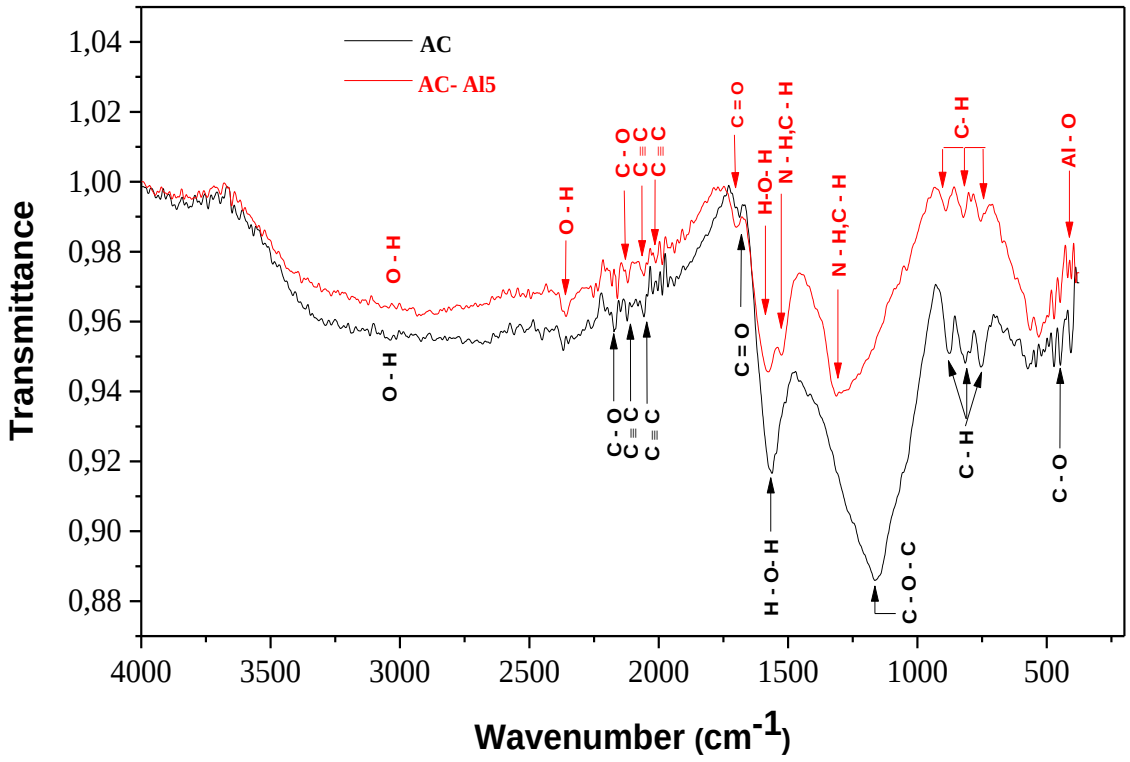
AC
AC- Al5
Transmittance
Wavenumber (cm-1)
1,04
1,02
1,00
0,98
0,96
0,94
0,92
0,90
0,88
4000
3500
3000
2500
2000
1500
1000
500
O - H
O - H
C - O
C ≡ C
C ≡ C
C ≡ C
C=O
H-O- H
N - H,C - H
N - H,C - H
C - H
Al - O
C=O
C - O
C ≡ C
C ≡ C
H - O - H
C - O - C
C - H
C - O

Fig. 2.

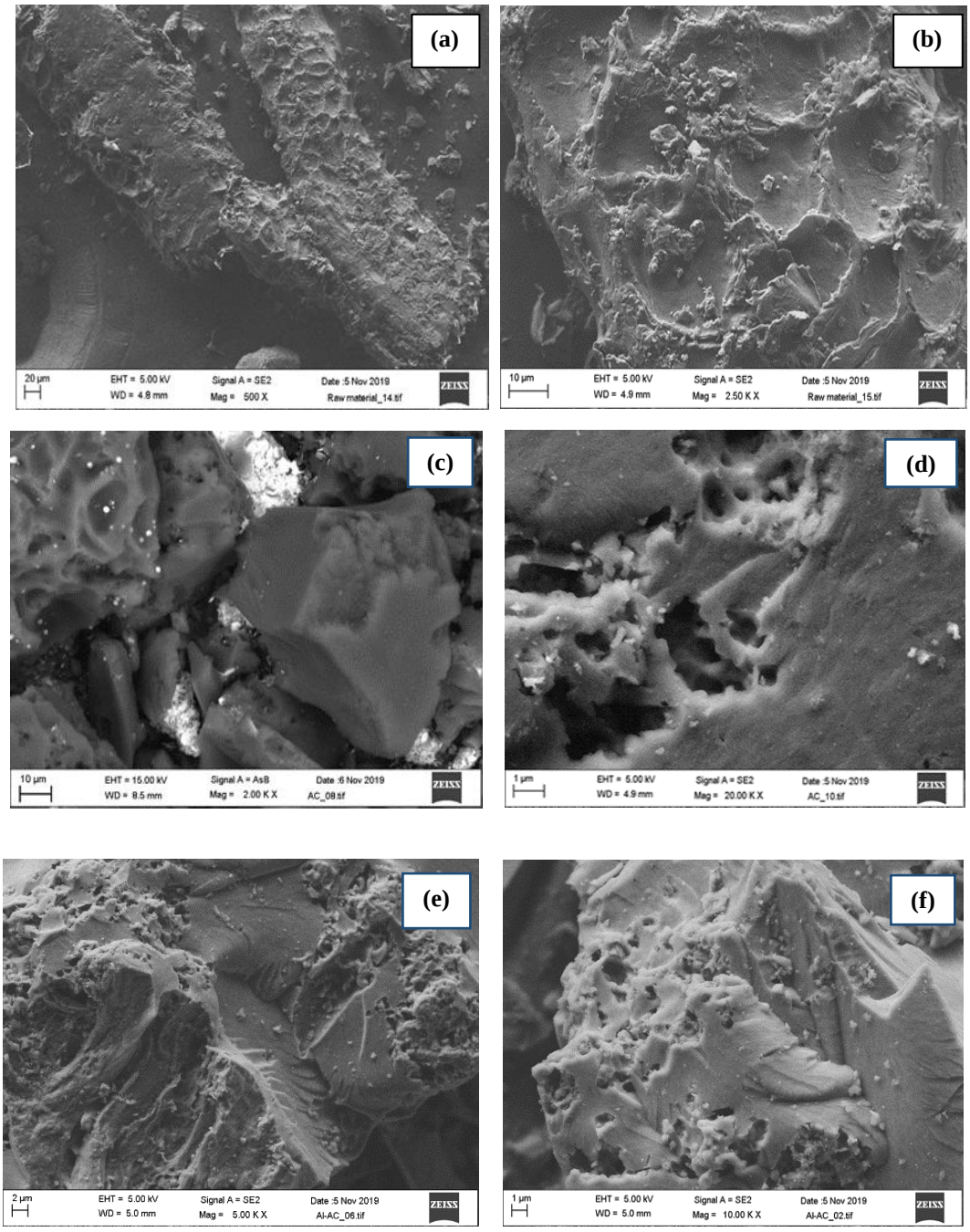
(a)
20 µm
EHT = 5.00 kV
WD = 4.8 mm
Signal A = SE2
Mag = 500 X
Date :5 Nov 2019
Raw material_14.tif
ZEISS
(b)
10 µm
EHT = 5.00 kV
WD = 4.9 mm
Signal A = SE2
Mag = 2.50 K X
Date :5 Nov 2019
Raw material_15.tif
ZEISS
(c)
10 µm
EHT = 15.00 kV
WD = 8.5 mm
Signal A = AsB
Mag = 2.00 K X
Date :6 Nov 2019
AC_08.tif
ZEISS
(d)
1 µm
EHT = 5.00 kV
WD = 4.9 mm
Signal A = SE2
Mag = 20.00 K X
Date :5 Nov 2019
AC_10.tif
ZEISS
(e)
2 µm
EHT = 5.00 kV
WD = 5.0 mm
Signal A = SE2
Mag = 5.00 K X
Date :5 Nov 2019
Al-AC_06.tif
ZEISS
(f)
1 µm
EHT = 5.00 kV
WD = 5.0 mm
Signal A = SE2
Mag = 10.00 K X
Date :5 Nov 2019
Al-AC_02.tif
ZEISS

Fig. 3.

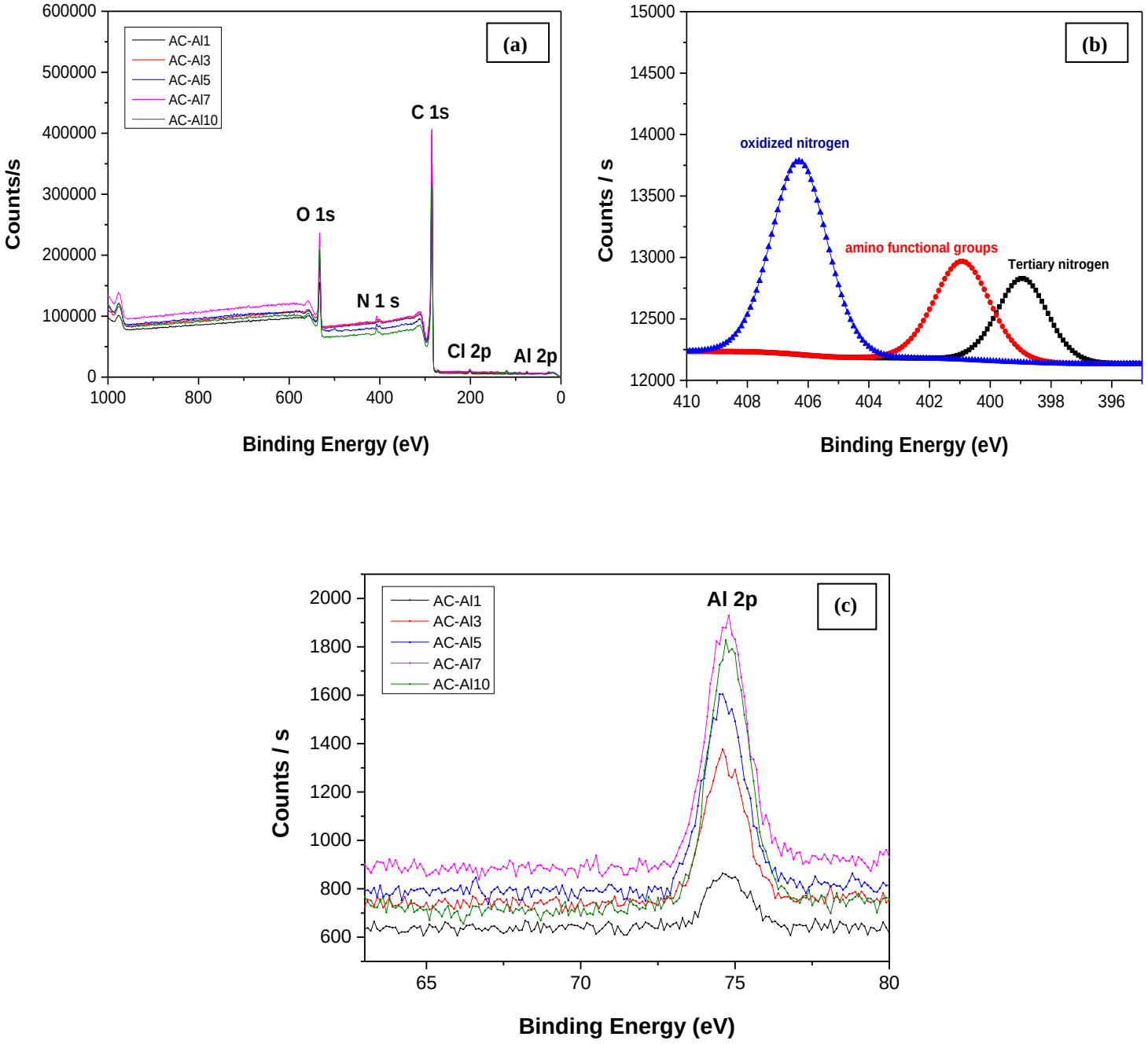
(a)
AC-Al1
AC-Al3
AC-Al5
AC-Al7
AC-Al10
C 1s
O 1s
N 1 s
Cl 2p
Al 2p
Counts/s
Binding Energy (eV)
(b)
oxidized nitrogen
amino functional groups
Tertiary nitrogen
Counts / s
Binding Energy (eV)
(c)
Al 2p
AC-Al1
AC-Al3
AC-Al5
AC-Al7
AC-Al10
Counts / s
Binding Energy (eV)

Fig. 4.

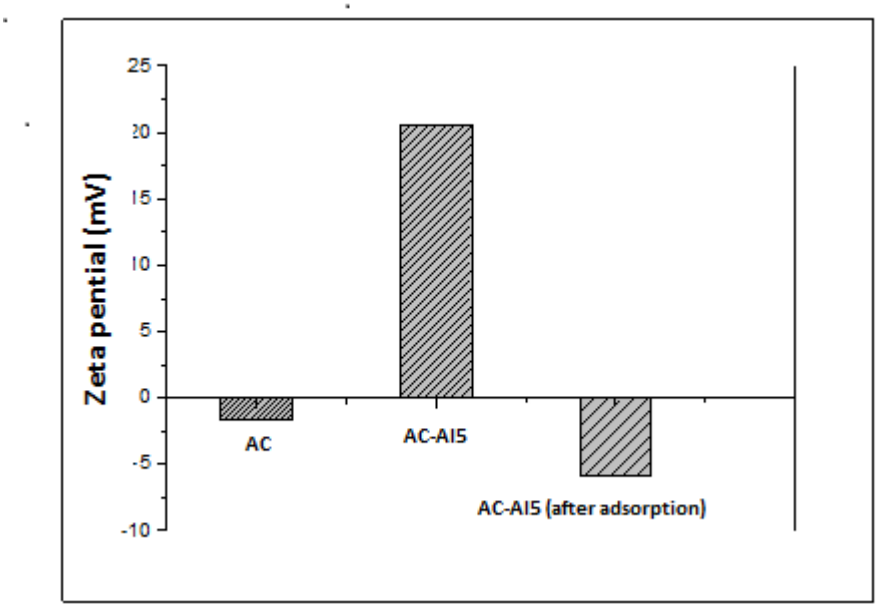
Zeta pential (mV)
25
20
15
10
5
0
-5
-10
AC
AC-AI5
AC-AI5 (after adsorption)

Fig. 5.

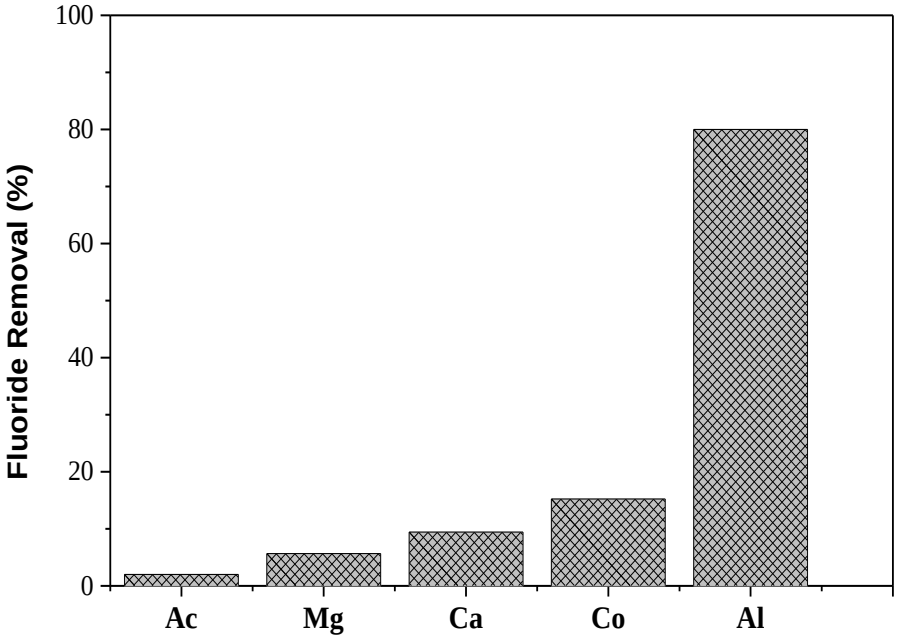
Fluoride Removal (%)
100
80
60
40
20
0
Ac
Mg
Ca
Co
Al

Fig. 6.

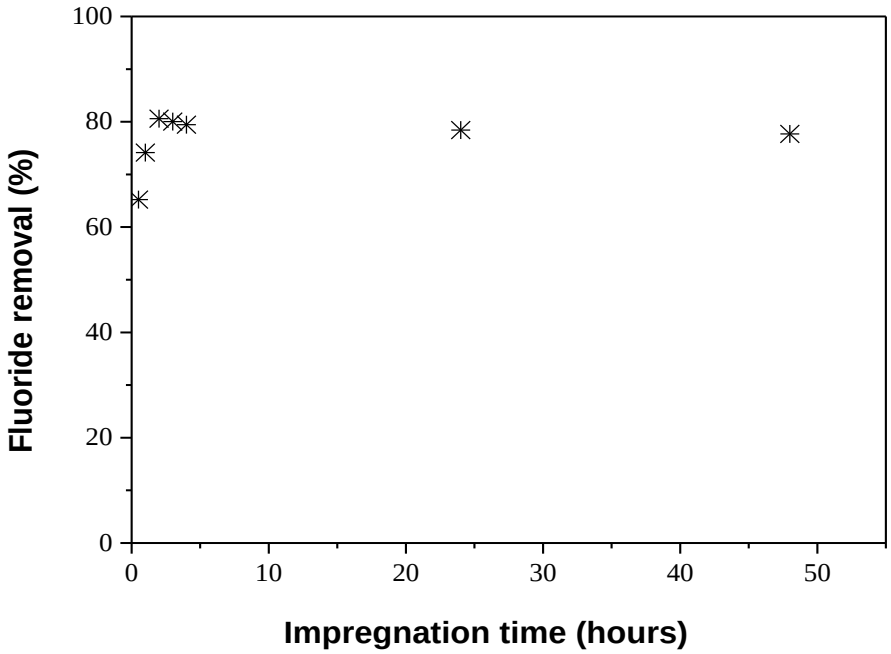
Fluoride removal (%)
Impregnation time (hours)
0
20
40
60
80
100
0
10
20
30
40
50

Fig. 7.

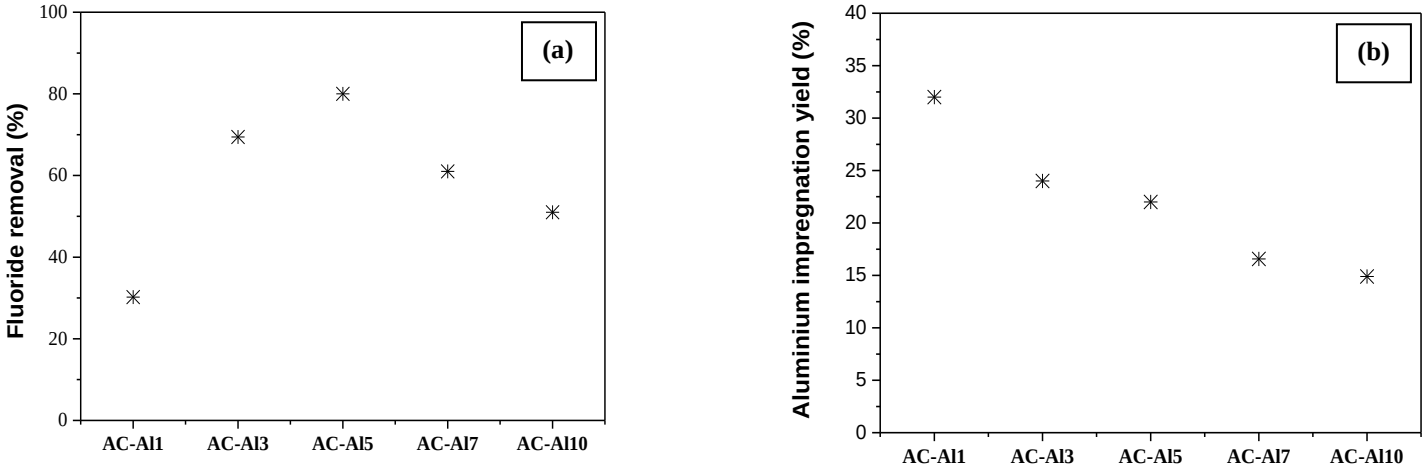
(a)
Fluoride removal (%)
AC-Al1
AC-Al3
AC-Al5
AC-Al7
AC-Al10
(b)
Aluminium impregnation yield (%)
AC-Al1
AC-Al3
AC-Al5
AC-Al7
AC-Al10

Fig. 8.

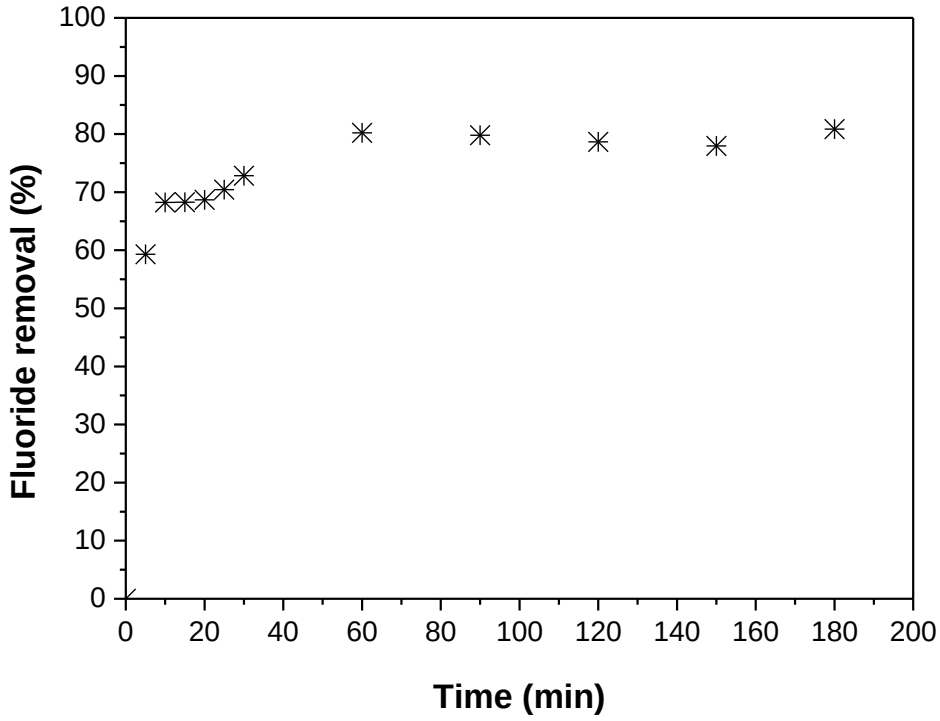
Fluoride removal (%)
Time (min)
0
10
20
30
40
50
60
70
80
90
100
0
20
40
60
80
100
120
140
160
180
200

Fig 9.

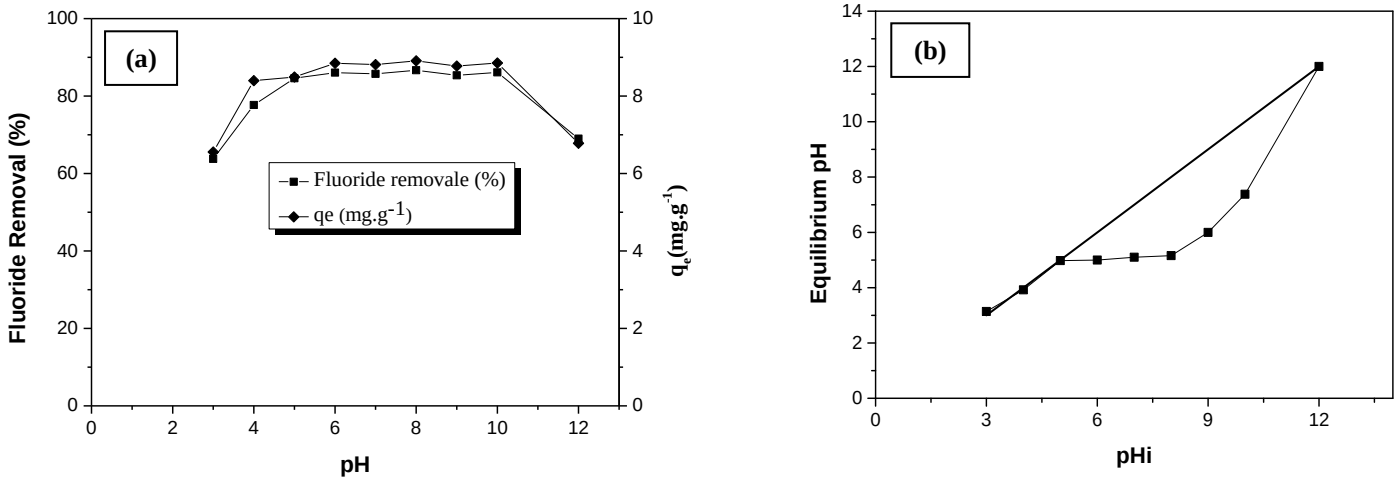
(a)
Fluoride Removal (%)
pH
Fluoride removale (%)
qe (mg.g-1)
qe(mg.g-1)
(b)
Equilibrium pH
pHi

Fig.10.

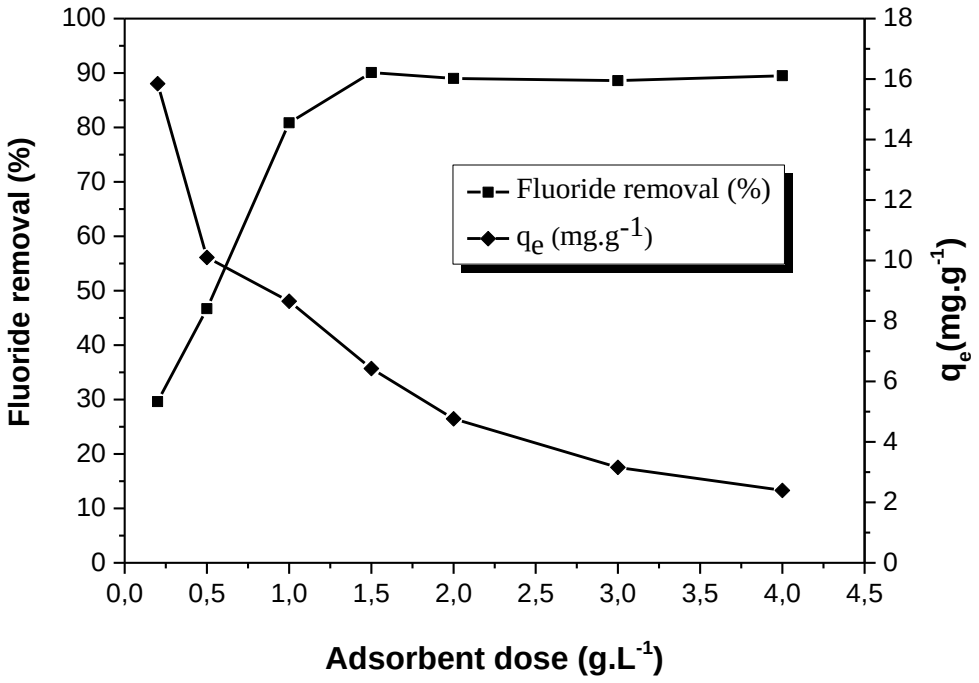
Fluoride removal (%)
q_e (mg.g^{-1})
Fluoride removal (%)
q_e(mg.g^{-1})
Adsorbent dose (g.L^{-1})

Fig.11.

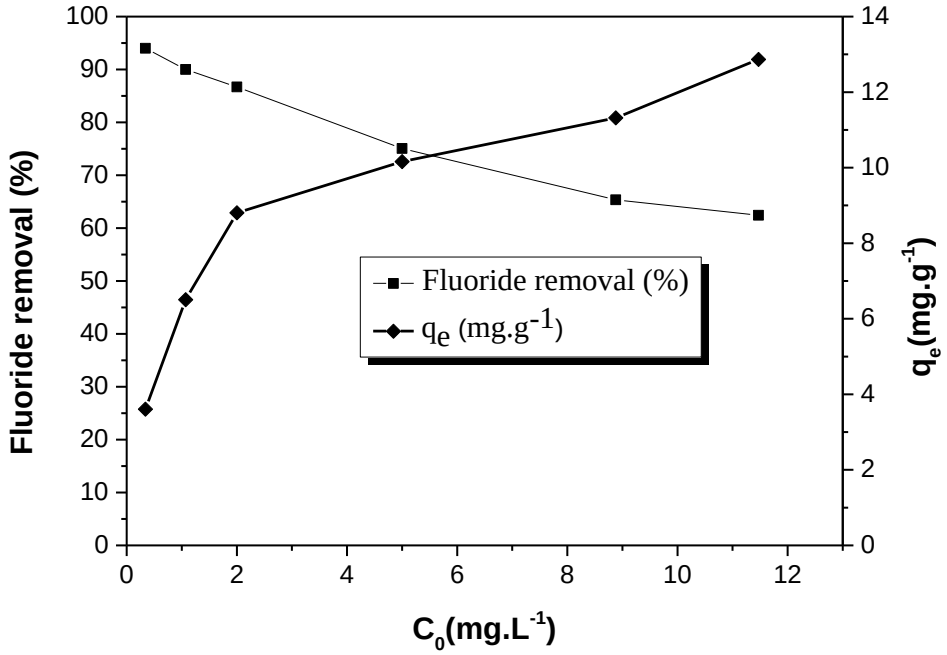
Fluoride removal (%)
q_e (mg.g^{-1})
Fluoride removal (%)
q_e(mg.g^{-1})
C_0(mg.L^{-1})

Fig.12.

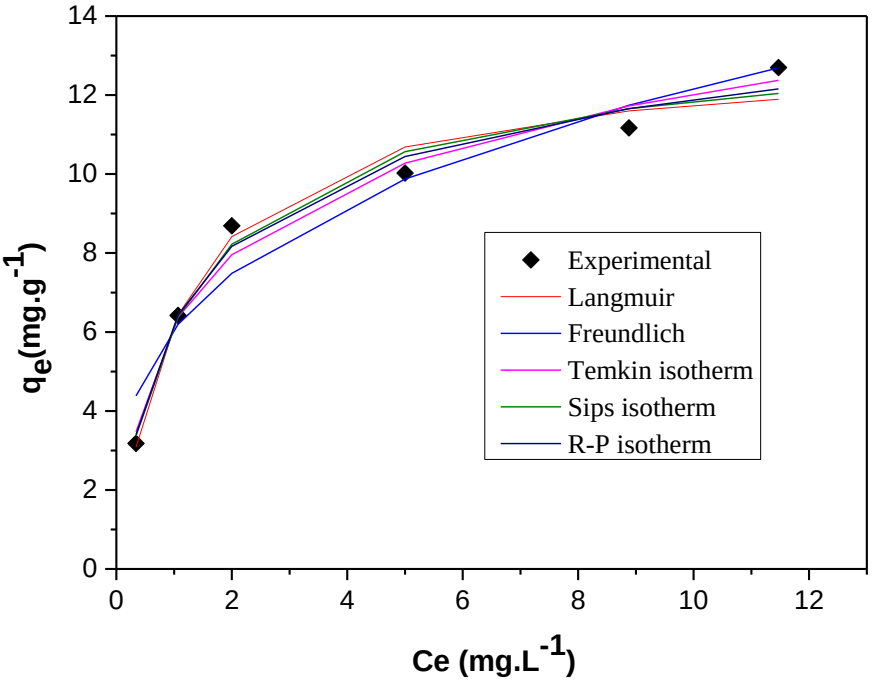

Fig. 13.

Fig. 1. Comparative XRD data for Activated carbons AC and Al-AC5.

Fig. 2. FTIR spectra of AC and AC-Al5.

Fig. 3. FESEM micrographs for (a, b) raw date stems, (c, d) AC and (e, f) AC-Al5.

Fig. 4. (a) XPS survey spectrum of AC-Al at different aluminum loading, (b) N 1s XPS spectrum of AC-Al5 and (c) Al 2p XPS spectrum of AC-Al at different aluminum loading.

Fig. 5. Zeta potential of AC, AC-Al5 and AC-Al5 (after adsorption)

Fig. 6. Results for fluoride removal of modified AC with different metal ions. (AC-Y) dose = 1 g, T = 25 °C, pH = 6.15, $[F^-]$ = 10 $mg.L^{-1}$.

Fig. 7. Effect of the impregnation time of the AC with Aluminum solution on the fluoride removal. (AC-Al5) dose = 1 g, T = 25 °C, pH = 6.15, $[F^-]$ = 10 mg L^{-1}.

Fig. 8. (a) Effect of the Aluminum loading on the fluoride removal during the AC impregnation and (b) effect of the Aluminium loading on aluminum impregnation yield. (AC-Al) dose = 1g, T = 25 °C, pH = 6.15, $[F^-]$ = 10 $mg.L^{-1}$.

Fig.9. Effect of contact time the fluoride removal. Adsorbent dose = 1 g, T = 25 °C, pH = 6.15, $[F^-]$ = 10 $mg.L^{-1}$.

Fig.10. (a) Effect of pH on the fluoride removal and (b) equilibrium pH after adsorption. Adsorbent dose = 1 g, T = 25 °C, $[F^-]$ = 10 $mg.L^{-1}$.

Fig.11. Effect of adsorbent dose on the fluoride removal. $[F^-]$ = 10 $mg.L^{-1}$, pH = 6.15, T = 25 °C.

Fig.12. Effect of initial concentration on the fluoride removal. T = 25 °C, pH = 6.15, Adsorbent dose = 1.5g.

Fig. 13. Comparative experimental and theoretical adsorption isotherms. Adsorbent dose = 1.5 g, pH = 6.15, T= 25 °C